Role of methane and biogenic volatile organic compound sources in late glacial and Holocene fluctuations of atmospheric methane concentrations

Jed Kaplan, Gerd Folberth, Didier Hauglustaine

Role of methane and biogenic volatile organic compound sources in late glacial and Holocene fluctuations of atmospheric methane concentrations

Jed O. Kaplan,[1] Gerd Folberth,[2] and Didier A. Hauglustaine[3]

Received 21 July 2005; revised 10 February 2006; accepted 24 February 2006; published 14 June 2006.

[1] Recent analyses of ice core methane concentrations suggested that methane emissions from wetlands were the primary driver for prehistoric changes in atmospheric methane. However, these interpretations conflict as to the location of wetlands, magnitude of emissions, and the environmental controls on methane oxidation. The flux of other reactive trace gases to the atmosphere also controls apparent atmospheric methane concentrations because these compounds compete for the hydroxyl radical (OH), which is the primary atmospheric sink for methane. In a series of linked biosphere-atmosphere chemistry-climate modeling experiments, we simulate the methane and biogenic volatile organic compound emissions from the terrestrial biosphere from the Last Glacial Maximum (LGM) to the present. Using a state-of-the-art chemistry-climate model, we simulate the atmospheric concentrations of methane, OH, and other reactive trace gas species. Over the past 21,000 years, methane emissions from wetlands increased slightly to the end of the Pleistocene but then decreased again, reaching levels at the preindustrial Holocene that were similar to the LGM. Global wetland area decreased by 14% from LGM to the preindustrial time. Emissions of biogenic volatile organic compounds (BVOCs), however, nearly doubled over the same period of time. Atmospheric OH burdens and methane concentrations were affected by this major change in BVOC emissions, with methane lifetimes increasing by more than 2 years from LGM to the present. We simulate a change in methane concentration of ~385 ppb, accounting for 88% of the ~440 ppb increase in methane concentrations observed in ice cores. Thus glacial-interglacial changes in atmospheric methane concentrations would have been modulated by BVOC emissions. In addition, the increase in atmospheric methane concentrations since the mid-Holocene is partly caused in our results by the increases in anthropogenic methane emissions over this period. While the interplay between BVOC and wetland methane emissions since the LGM cannot explain the entire record of ice core methane concentrations, consideration of BVOC source dynamics is central to understanding ice core methane. Rapid changes in atmospheric methane concentrations, also observed in ice cores, require further study.

Citation: Kaplan, J. O., G. Folberth, and D. A. Hauglustaine (2006), Role of methane and biogenic volatile organic compound sources in late glacial and Holocene fluctuations of atmospheric methane concentrations, *Global Biogeochem. Cycles*, *20*, GB2016, doi:10.1029/2005GB002590.

1. Introduction

[2] Over at least the past 400 ka, atmospheric methane (CH_4) concentrations have fluctuated between approximately 350 ppb in the coldest glacial stages and 750 ppb in warm periods [*Petit et al.*, 1999]. CH_4 concentrations measured in gas bubbles preserved in polar ice show that over this time period, fluctuations in atmospheric CH_4 concentrations were rapid, on the order of a century, and of high magnitude, sometimes increasing by several hundred ppb [*Brook et al.*, 1996]. Furthermore, the CH_4 record more closely parallels the higher-frequency component of polar temperature records than any other measured trace gas. To explain the variability in atmospheric CH_4 concentrations from the Last Glacial Maximum (LGM, circa 21 ka) to the latest preindustrial Holocene (PIH, circa 1850) remains an elusive scientific task [*Valdes et al.*, 2005].

[3] As a reactive trace gas with a limited lifetime in the atmosphere, changes in atmospheric CH_4 concentrations may be due either to (1) variations in the magnitude of

[1]Institute of Plant Sciences, University of Bern, Bern, Switzerland.
[2]School of Earth and Ocean Sciences, University of Victoria, Victoria, British Columbia, Canada.
[3]Laboratoire des Sciences du Climat et de l'Environnement, Gif-sur-Yvette, France.

0886-6236/06/2005GB002590

CH_4's mainly terrestrial sources and or (2) variations in the magnitude of its primary sink: reaction with the hydroxyl radical (OH) in the troposphere. Therefore changes in atmospheric CH_4 concentrations are likely to be diagnostic of changes in the Earth system. Because of the potency of CH_4 as a greenhouse gas – it is responsible for ~17% of the total trace gas–induced atmospheric radiative forcing at present [*Ramaswamy et al.*, 2001] – an understanding of the natural controls on CH_4 formation and destruction is crucial for predicting the role of CH_4 in future climate change.

[4] Several competing theories have been proposed to explain the observed rapid changes in atmospheric CH_4 concentrations, including changes in wetland area and productivity or catastrophic releases of CH_4 hydrates from the oceans [*Brook et al.*, 2000; *Dällenbach et al.*, 2000; *Kennett et al.*, 2003]. Regardless of the cause, the lifetime of CH_4 in the atmosphere is relatively short, on the order of a decade, so a fundamental change in the nature of the global CH_4 cycle, either in sources or in sinks, must be considered to explain the observed millennial-scale changes in atmospheric CH_4.

[5] Mechanisms to explain glacial-interglacial-scale variability in atmospheric CH_4 concentrations are fewer, but recent analyses of ice core CH_4 concentrations, interhemispheric gradients, and carbon isotope composition ($\delta^{13}C$-CH_4) have suggested that changes in CH_4 emissions from wetlands drove prehistoric changes in ice core CH_4 [*Chappellaz et al.*, 1993b, 1997; *Crutzen and Bruhl*, 1993; *Martinerie et al.*, 1995; *Schaefer*, 2005]. The theory has been that a glacial world, with its relatively cold oceans would have been drier than the present, and reduced global wetland area would lead to a suppression in the largest natural source of CH_4. Additionally, the presence of large Northern Hemisphere ice sheets may have led to a reduction in the area of boreal wetlands, and lower atmospheric CO_2 concentrations led to reduced productivity of global vegetation. Both of these factors would also have had a generally negative effect on CH_4 emissions. However, results of recent modeling work using global biochemical process models, indicated that glacial-interglacial changes in wetland area and CH_4 emissions may have been smaller than earlier supposed, and possibly not large enough to effect the observed changes in atmospheric CH_4 concentrations [*Adams et al.*, 2001; *Kaplan*, 2002; *Valdes et al.*, 2005].

[6] Both process-based "bottom-up" modeling studies and "top-down" interpretations of ice core CH_4 concentrations have focused on changes in CH_4 sources to explain the long-term changes in atmospheric CH_4 concentrations [*Kaplan*, 2002]. These approaches have mostly neglected the possibility that CH_4 sinks could also have changed in magnitude on glacial-interglacial cycles, and may omit an important part of the global CH_4 budget. *Adams et al.* [2001] speculated that large changes in atmospheric CH_4 concentrations could be effected through changes in the emissions of reactive volatile organic compounds (RVOCs). A recent bottom-up modeling analysis of ice age and preindustrial CH_4 budgets that included changes in the sources of other reactive trace gases concluded that changes in RVOC emissions could explain much of the glacial-interglacial difference in atmospheric CH_4 concentrations [*Valdes et al.*, 2005].

[7] RVOCs include isoprene, terpenes, acetone, and methanol, as well as numerous other short-lived compounds. These compounds have their primary sink in the troposphere through reaction with the hydroxyl radical (OH), which is also the main sink for CH_4. Because of this "competition" for the OH sink, variations in the magnitude of RVOC sources could cause changes in the apparent concentration of CH_4. Variations in natural RVOC emissions may have occurred not only on glacial-interglacial timescales, but also throughout the Holocene, with consequences for atmospheric CH_4 concentrations and the atmospheric radiative budget.

[8] Following the hypotheses advanced in the empirical study of *Adams et al.* [2001], we investigate the potential importance of changing RVOC emissions on the magnitude of the OH sink and consequent atmospheric CH_4 concentrations. By using a series of paleoclimate scenarios performed by a GCM as a basis for global terrestrial vegetation model simulations of vegetation and wetland distributions, we calculate CH_4 emissions from wetlands, and biogenic RVOC emissions from terrestrial vegetation. With this inventory of surface fluxes, we conduct a set of 3D atmospheric chemistry transport model runs to simulate the lifetime of atmospheric CH_4 at four key time slices during the past 21 ka. Analysis of the results allows us to speculate on the potential long-term controls on CH_4 concentrations at the LGM, early Holocene, mid-Holocene, and preindustrial period.

[9] By using a linked set of models that contain a quantitative representation of the physical, chemical and biological processes involved in the production and destruction of CH_4 at each step in its cycle, we are able to go beyond *Adams et al.* [2001] and directly simulate atmospheric CH_4 concentrations. Our work builds upon the process modeling work of *Valdes et al.* [2005] with novel simulations of CH_4 and BVOC emissions from the entire time period between the LGM and preindustrial, and includes direct estimates of CH_4 concentrations at the early and mid-Holocene, critical periods for examining early anthropogenic influence on greenhouse gas concentrations [*Ruddiman and Thomson*, 2001].

2. Methods and Model Description

[10] The method used in this study incorporates a stepwise, offline coupling of several models (Figure 1). A global climate model (UM-GCM) was used to simulate paleoclimate at 1 ka intervals from the LGM to the present. This GCM output was used by a global vegetation model (BIOME4-TG) to calculate vegetation distribution (biomes), wetland area, CH_4 emissions from wetlands, and BVOC emissions from the terrestrial vegetation. The surface flux fields of CH_4 and BVOC from BIOME4-TG were used as forcings for an atmospheric chemistry-climate model (LMDz-INCA). Using this combination of models, we were able to make an idealized 3D synthesis of the global CH_4 cycle and simulate CH_4 lifetime. From this, we estimate

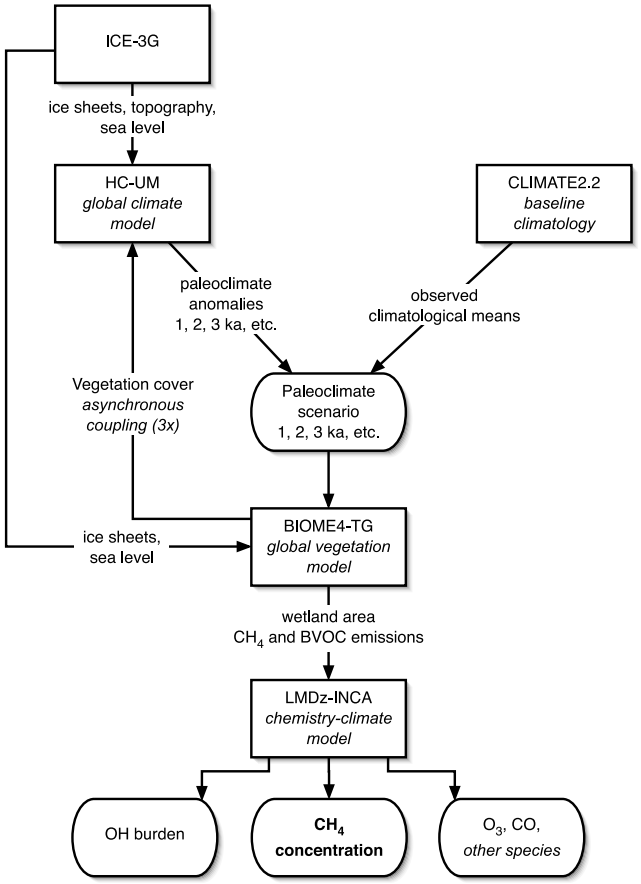

Figure 1. Schematic flowchart of the model coupling methodology used to simulate paleoatmospheric CH_4 concentrations.

atmospheric CH_4 concentrations and compare these results to ice core measured [CH_4].

2.1. Choice of Time Slices

[11] Although the surface fluxes produced by BIOME4-TG were available at every 1 ka time slice from 21 ka to 0 ka, computational requirements limited our selection of time slices for the LMDz-INCA simulations to four key periods in the past: LGM (21 ka), early Holocene (10 ka), mid-Holocene (6 ka), and preindustrial conditions (0 ka). This preindustrial control simulation represents potential natural conditions, without the impact of anthropogenic land use or emissions from fossil fuel use. The selected paleoclimate time slices for the chemistry-climate model experiments were chosen because these periods are the focus of modeling efforts in the Paleoclimate Model Intercomparison Project II (PMIP II) [*Harrison et al.*, 2002], and because they represent extremes in climate forcing.

[12] At the LGM, the Earth's orbital configuration was similar to today but the continental ice sheets were at a maximum and greenhouse gas concentrations were at a minimum [*Dyke and Prest*, 1987; *Raynaud et al.*, 1993; *Svendsen et al.*, 2004]. In addition to the large changes in terrestrial geography, the ocean surface was colder and the distribution of sea ice was greatly expanded compared to the present [*CLIMAP Project Members*, 1976, 1981]. The configuration of the Earth's orbit was substantially different from today or the LGM during the intervening period of the early to mid-Holocene. The phasing of the precession (19 kyr, 23 kyr) and obliquity (41 kyr) cycles was such that at the early Holocene (circa 11 ka) the high latitudes of the Northern Hemisphere received more insolation than any other time over the past 21 ka, both during summer and annually [*Berger et al.*, 1993]. At 10 ka, the northern high-latitude insolation was near its maximum; at 6 ka this effect was still significant but somewhat smaller. As a direct consequence of the orbital forcing, parts of the northern high latitudes experienced summers in the early and mid-Holocene that were considerably warmer than the present [*Bigelow et al.*, 2003; *MacDonald et al.*, 2000; *Ritchie et al.*, 1983].

[13] Other boundary conditions were different between 10 ka and 6 ka: the Laurentide ice sheet, although substantially reduced from its LGM size, was still sufficiently large to have a major downwind cooling effect during the early Holocene [*Harrison et al.*, 1992; *Mitchell et al.*, 1988]. At 10 ka, a residual Fennoscandian ice sheet also persisted in northern Europe, and sea level was ~30 m lower compared to 6 ka. Thus northern Europe and eastern North America experienced a thermal maximum several thousand years after the insolation maximum. In contrast, atmospheric greenhouse gases (CO_2, CH_4, and N_2O) had reached near preindustrial concentrations by 10 ka [*Raynaud et al.*, 1993], though they continued to fluctuate through the Holocene [*Indermühle et al.*, 1999].

2.2. BIOME4-TG Vegetation Model

[14] BIOME4-TG is an equilibrium-state terrestrial biosphere model that couples biogeography and biogeochemistry and is able to calculate the vegetation distribution at any time in the past or future in response to both changing climate and atmospheric CO_2 concentrations. The model is driven by monthly climatological mean temperature, precipitation, and solar radiation [*Kaplan*, 2001]. BIOME4-TG simulates both vegetation structure in the form of 28 world biomes, and a suite of standard biogeochemical variables, including NPP, LAI, autotrophic and heterotrophic respiration, water runoff, and soil moisture. The biomes in BIOME4-TG are defined so as to be downward compatible with the classification used in the BIOME 6000 data set of reconstructed past vegetation [*Prentice et al.*, 2000; *Prentice and Webb*, 1998]. BIOME4 has been used extensively for simulating past vegetation distributions and evaluating paleoclimate simulations by GCMs [*Harrison*, 2000; *Kaplan et al.*, 2003].

[15] BIOME4-TG extends the functionality of BIOME4 by including modules to simulate wetland area, CH_4 emissions from wetlands, and BVOC emissions from all vegetation types. To determine wetland area, BIOME4-TG uses simple algorithms based on topography and soil moisture; CH_4 emissions are based on ecosystem carbon turnover in wet soils [*Christensen et al.*, 1996; *Kaplan*, 2002]. Biogenic VOC emissions are calculated in BIOME4-TG on the basis

of algorithms from the Global Model of Natural Volatile Organic Compound Emissions [*Guenther et al.*, 1995].

2.3. Climate Scenarios Used by BIOME4-TG

[16] Paleoclimate scenarios used by BIOME4-TG were prepared by combining a GCM paleoclimate simulation with a baseline climatology of 20th century mean climate. Paleoclimate simulations were performed with the Hadley Centre Unified Model (HC-UM), including a model of the ocean mixed layer (''slab ocean'') [*Kaplan et al.*, 2002]. The paleoclimate scenarios were produced by applying climate anomalies, that is, differences in monthly mean climates between the HC-UM paleoclimate and control (''present-day'') simulations, to a ''baseline'' representing late 20th century mean climate. The HC-UM simulations were performed at 1000-year intervals from 21 ka to ''0 ka'' (preindustrial time). Boundary conditions for the climate simulations were orbital forcing, physiography (orography, ice sheets, sea level), and atmospheric CO_2 concentration. Land surface conditions (vegetation type, density, height, roughness, and phenology), including potential vegetation feedbacks to the climate system, were calculated through asynchronous coupling to the BIOME4 model [see, e.g., *de Noblet et al.*, 1996; *Kaplan*, 2006]. Because of the 1000-year time slice approach of the GCM simulations, rapid climate change events, for example, the Younger Dryas and 8.2 ka event, could not be taken into account in the paleoclimate scenarios. While these transient phenomena are of great interest in interpreting the ice core record of atmospheric CH_4, we limit our analysis to the longer-term changes in the CH_4 cycle, which we hypothesize to be affected by different processes.

[17] BIOME4-TG was run on a $0.5^\circ \times 0.5^\circ$ geographic grid, corresponding to the resolution of the baseline climatology. The CLIMATE 2.2 baseline climatology is a gridded long-term mean climatology for the 20th century that includes monthly mean temperatures and percent of potential sunshine hours, and monthly total precipitation [*Kaplan et al.*, 2003; *Leemans and Cramer*, 1991]. The grid includes all ''virtual'' land grid cells on the continental shelf areas that were exposed at the LGM and times between then and the present. The land and ice mask at each 1 ka interval was defined by a series of simulations from the dynamic ice sheet–crustal deformation model ICE-3G [*Peltier*, 1994]. The ICE-3G output was linearly interpolated from its native 1° grid to the 0.5° grid used by BIOME4-TG.

[18] An atmospheric CO_2 concentration of 324 ppm was used to force BIOME4-TG for the present-day simulation. This value represents the mean $[CO_2]$ during the period of measurement of the station data upon which the climatology is based. For paleoclimate simulations, CO_2 concentrations were interpolated at 1 ka intervals from the Taylor Dome and Byrd Antarctic ice core CO_2 records [*Neftel et al.*, 1988; *Indermühle et al.*, 1999; *Stauffer et al.*, 1998].

2.4. LMDz-INCA Atmospheric Chemistry-Climate Model

[19] LMDz (Laboratoire de Météorologie Dynamique, zoom) is a full complexity, 3D General Circulation Model (GCM) initially developed for climate studies by *Sadourny and Laval* [1984]. As part of the IPSL Earth System Model, the GCM has been applied in land surface–climate feedback studies by *Friedlingstein et al.* [2001] and *Dufresne et al.* [2002]. In LMDz the finite volume transport scheme of *Van Leer* [1977] is used to calculate large-scale advection of tracers and deep convection is parameterized according to the scheme of *Tiedke* [1989]; a local second-order closure formalism has been integrated to describe turbulent mixing in the planetary boundary layer (PBL). LMDz (version 3.3) has a horizontal resolution of 3.8×2.5 degrees on the horizontal and uses 19 vertical σp levels extending from the surface to 3 hPa.

[20] The Interactive Chemistry and Aerosols (INCA) model has been integrated into LMDz. INCA includes 83 chemical species, 43 photolytic reactions, and 217 thermochemical reactions. INCA has been designed to simulate tropospheric chemistry, emissions, and deposition of primary trace species of the troposphere including non-CH_4 hydrocarbons (NMHC) and non-CH_4 volatile organic compounds (NMVOC). Detailed description and evaluation of LMDz-INCA and emission inventories can be found in *Hauglustaine et al.* [2004], *Folberth et al.* [2005a, 2005b], and *Lathière et al.* [2005].

2.5. Emission Inventories

[21] In order to represent preindustrial conditions, the surface emission magnitude for several species in the standard LMDz-INCA emission inventory, which is characteristic for the present-day environment, had to be readjusted. Modifications follow the representative inventory for the year 1850 of *Lelieveld et al.* [1998] for most species, with *Yienger and Levy* [1995] for NO_x. The changes include the elimination of all surface emissions from fossil fuel combustion, a reduction of the biomass burning emissions (including agricultural waste burning and fuel wood use) for all species to 15% of their present-day magnitude, and a decrease in the NO_x soil emissions to 2.9 Tg N yr^{-1} (as opposed to 5.5 Tg N yr^{-1} for the present). The global atmospheric NO_x source from lightning was kept at its present-day value of 5.0 Tg N yr^{-1}. CH_4 emissions from rice paddies, wild animals and ruminants, and landfills (not included in BIOME4-TG) were set to 33% (19.7 Tg C yr^{-1}), 29% (20.3 Tg C yr^{-1}), and 25% (6.7 Tg C yr^{-1}), respectively, of their present-day magnitude, following *Lelieveld et al.* [1998].

[22] BIOME4-TG simulated inventories of wetland CH_4 and biogenic isoprene, terpenes, and other reactive volatile organic compounds (ORVOC). Because LMDz-INCA requires surface fluxes of individual VOC species as input, the geographic distribution of all species other than isoprene and terpenes was determined by the simulated distribution of total ORVOC. Emission magnitude was determined by rescaling the standard emission inventory for each species by the total ORVOC flux simulated by BIOME4-TG at each time slice. In other words, we assume a linear relationship between total ORVOC emissions and the emissions of any given species; an assumption that, in view of the lack of any other information, seems reasonable. Table 1 summarizes the emission inventories for the key species as used in this study.

Table 1. LMDz-INCA Emission Inventory as Used in the Time Slice Experiments[a]

	LGM (21 ka) Emissions	10 ka		6 ka		PI (0 ka)	
		Emissions	Percentage Change	Emissions	Percentage Change	Emissions	Percentage Change
NO_x	9.3	9.3	—	9.3	—	9.3	—
CH_4	150.9	162.9	+8	146.2	−3	179.3	+19
CO	61.1	61.1	—	61.1	—	85.4	+40
Isoprene	335.3	538.5	+61	516.4	+54	540.7	+61
Terpenes	80.3	112.1	+40	117.6	+46	121.3	+51
Methanol	70.7	106.4	+50	106.5	+51	112.7	+59
Acetone	37.1	49.5	+33	49.5	+33	51.6	+39
$\sum$ other VOC	14.3	17.9	+25	17.9	+25	18.5	+29
Total RCC	749.7	1048.3	+40	1015.2	+35	1109.4	+48

[a]NO_x emissions are given in Tg N yr^{-1}, and reactive carbon compound (RCC) emissions are given in Tg C yr^{-1}. Percent values indicate an increase in the surface sources relative to their magnitudes at LGM.

[23] In the three paleo time slice experiments it was assumed that the remaining anthropogenic portion of preindustrial surface RVOC emissions did not yet exist. This includes CH_4 emissions from rice paddies and landfills, and CO emissions from agricultural waste burning and fuel wood use. CH_4 emissions from ruminants were kept at their preindustrial magnitude. The elimination of anthropogenic emissions amounts to approximately 15% and 30% of the total preindustrial fluxes of CH_4 and CO respectively, but in each case constitute only slightly more than 2% of the total preindustrial RCC emission magnitude of ~1110 TgC yr^{-1}. We do not consider our emission inventories to be an exact representation of the conditions at the four time periods considered here, but rather a rough estimate based on many assumptions, which nevertheless seem reasonable in view of the present knowledge and the purpose of this study.

2.6. Experiments Performed by LMDz-INCA

[24] At the four time slices described above, we ran LMDz-INCA to calculate OH burdens, and CH_4 lifetime and concentrations. While the emission inventories of CH_4 and BVOC simulated by BIOME4-TG varied geographically with changing sea level and ice sheet conditions, all other forcings on LMDz-INCA were held constant in order to specifically assess the role played by changing surface emissions on atmospheric CH_4 concentrations.

[25] The boundary conditions affecting the physical climate, including insolation and land and sea ice distributions, were fixed to preindustrial conditions in each LMDz-INCA experiment. This resulted in similar temperatures, winds, water vapor, and surface albedo simulated by the chemistry-climate model. The stratospheric ozone column was also kept constant between the time slices.

[26] Each simulation was initialized by a set of restart conditions from a previous model run and was taken over a 30 months period to allow a new equilibrium state in reactive trace gas concentrations to be reached. To facilitate an estimation of the photochemical equilibrium for CH_4 – this would otherwise take approximately 20 model years – the CH_4 field was globally initialized to a value close to the expected equilibrium concentration. The global mean CH_4 concentration was closely monitored and found to be in equilibrium within reasonable limits (continuous increase or decrease in CH_4 of less than 5% from year 1 to year 2) in all four cases. The change in the global annual mean CH_4 concentration from year 1 to year 2 amounts to 0.5%, −0.1%, 1.1%, and 3.1% for the PI, 6 ka, 10 ka, and LGM run, respectively.

[27] Interannual variability in these runs is expected to be on the order of 0.5 to 1% for both global mean CH_4 concentration and OH burden. Hence a substantial amount of the change between year 1 and year 2 can be explained by the model's interannual climate variability, which was assessed by analyzing a four model−year record of control runs for present-day conditions. All other species have photochemical lifetimes sufficiently short to reach equilibrium well within six model months. The last 12 months of each run were selected for analysis.

[28] The boundary conditions and model setup described above have significant implications for the modeled global distribution of OH and consequently for CH_4 concentrations. Uncertainties resulting from this modeling approach are discussed fully in the results section.

3. Results and Discussion

3.1. Vegetation Distribution

[29] Qualitative comparison of global vegetation distribution simulated in our control "preindustrial" simulation (Figure 2a) with modern observations, descriptive accounts of presettlement vegetation, paleodata synthesis, and recent modeling studies yields good agreement in most parts of the world [*Haxeltine and Prentice*, 1996; *Prentice and Webb*, 1998; *Walter*, 1973]. Boreal, temperate, and tropical forests occupy areas near their observed limits along with deserts and tropical savannas. BIOME4-TG, similar to other global vegetation models, systematically fails to reproduce observed vegetation distribution at locations where it underestimates the area of grassland and temperate savannah in favor of forest, for example, in central North America and the South American pampas [*Sitch et al.*, 2003]; the model also overestimates the area of forest in hypermaritime boreal regions [*Kaplan et al.*, 2003]. These biomes may be the result of processes including long-term regular disturbance or extreme diurnal variability in meteorological conditions [*Transeau*, 1935; *Walter et al.*, 1975], processes that are not incorporated in BIOME4-TG. On the long timescales in-

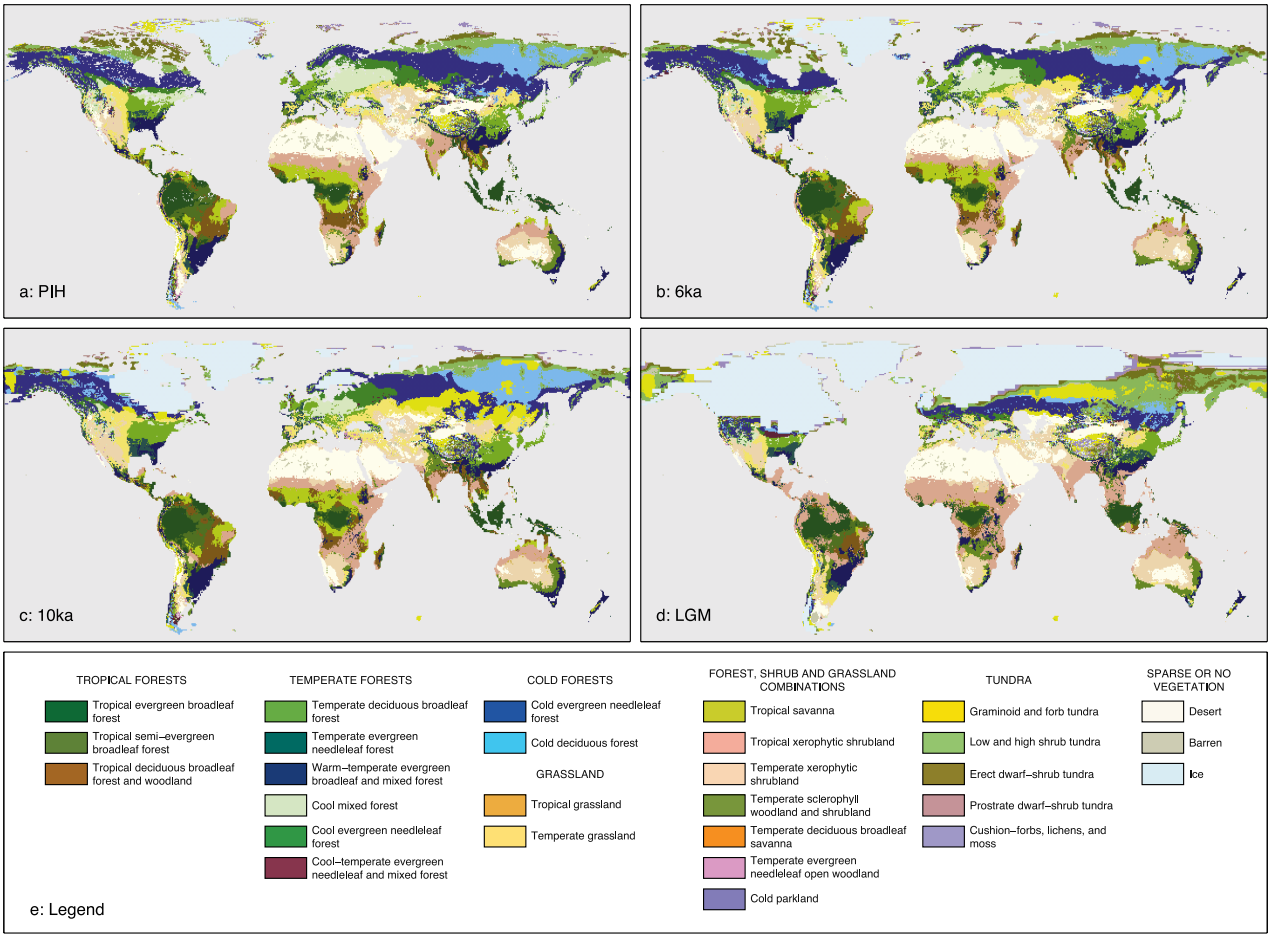

Figure 2. Biomes simulated by BIOME4-TG at (a) the "preindustrial" (0 ka), (b) 6 ka, (c) 10 ka, and (d) LGM (21 ka). (e) Legend for all biome types simulated by BIOME4-TG.

vestigated in this study, however, shifts in global vegetation were much larger than the uncertainty associated with the simulation of present-day distributions [*Prentice*, 2001]. Over the past 21 ka global vegetation distribution responded to the melting ice sheets, rising sea level, changing climate and increasing atmospheric CO_2 concentrations that accompanied deglaciation (Figures 2b, 2c, and 2d).

[30] Large ice sheets, tundra, and xeric herbaceous and scrub vegetation dominated the LGM landscape (Figure 2d). The LGM simulation shows the prevalence of graminoid and forb tundra in Siberia and on the Bering land bridge at the LGM that are observed in paleoecological reconstructions of vegetation during this time [*Bigelow et al.*, 2003]. With no widespread modern analog, the graminoid and forb tundra is indicative of very cold and dry climate conditions that favor herbaceous vegetation over shrubs. As both paleodata synthesis and other modeling studies have suggested, significant areas of tropical rain forest persisted at the LGM, particularly in the most humid areas of the Sunda shelf, and Amazon and Congo basins [*Cowling et al.*, 2001; *Hope et al.*, 2004; *Prentice et al.*, 2000]. Otherwise, the tropics are dominated by xerophytic scrub vegetation, which may have occurred as a consequence of cool temperatures, low CO_2, or a combination of the two [*Jolly and Haxeltine*, 1997].

[31] During the early and mid-Holocene (10 ka and 6 ka time slices), boreal regions are characterized by a large increase in the area of forest compared to LGM (Figures 2b and 2c). The Eurasian boreal forest reaches its farthest northern extent at 10 ka, coincident with the summertime insolation maximum at this time. Further south in central Siberia the same time period is marked by the persistence of graminoid and forb tundra in the model simulation. While perhaps not a classically defined tundra under these 10 ka conditions, this biome type is nonetheless indicative of the cold, xeric, and low-productivity environment. In North America, the persistence of the Laurentide ice sheet prevented the boreal forest from reaching its maximum northward extent until circa 6 ka. Tropical vegetation developed to conditions similar to the present already by the early Holocene, and at both 10 ka and 6 ka forests indicative of a more humid climate compared to preindustrial developed in South Asia because of the intensified summer monsoon. In contrast, the Sahara desert region does not show the shift in

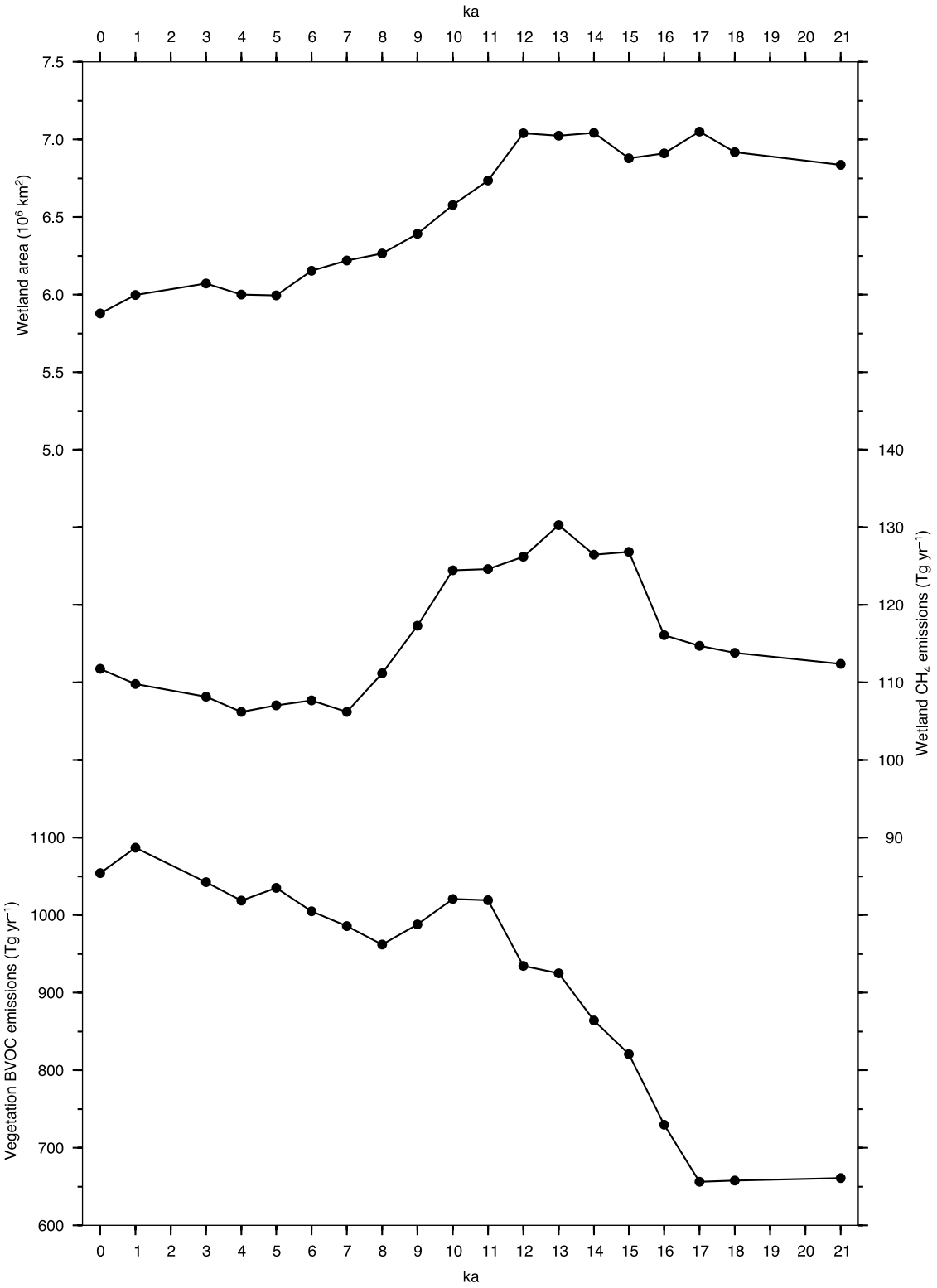

Figure 3. Wetland area, CH_4 emissions, and BVOC emissions simulated by BIOME4-TG at each of the 1000-year paleoclimate scenario time slices.

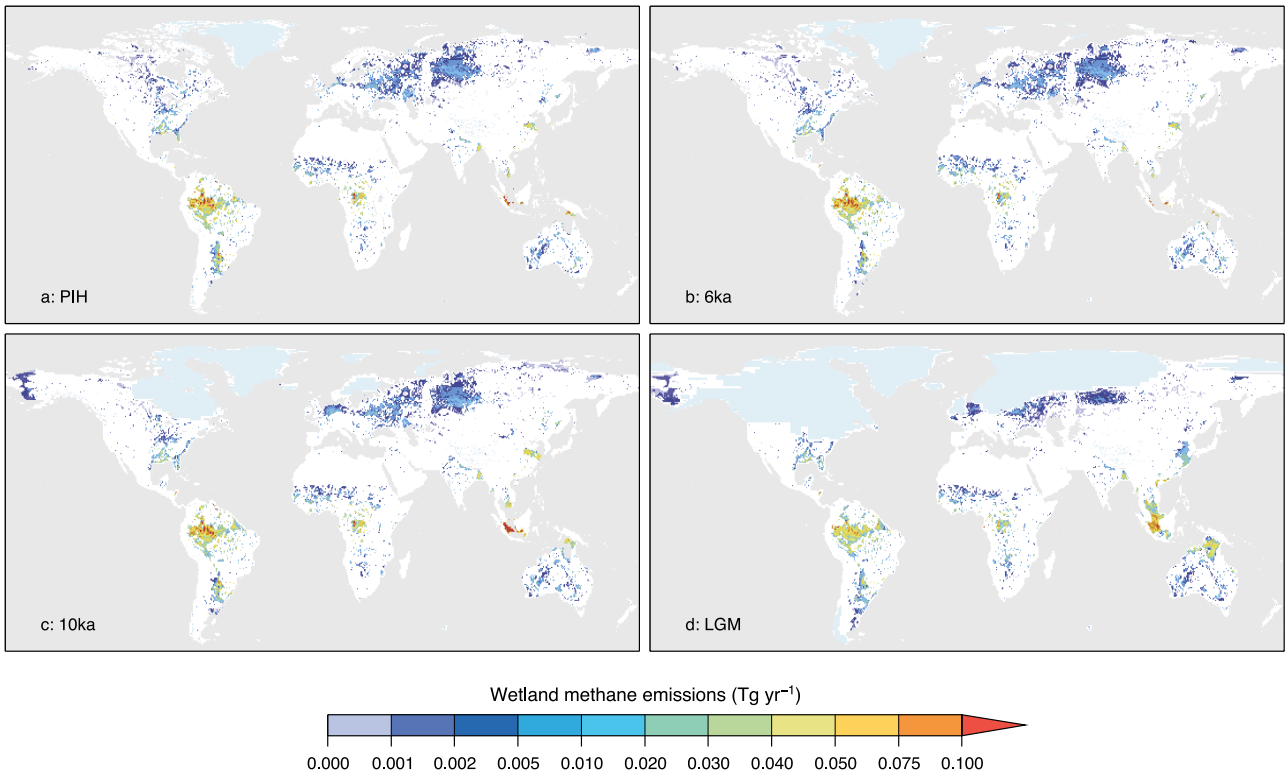

Figure 4. Global distribution of total annual CH_4 emissions from wetlands simulated by BIOME4 at (a) the "preindustrial" (0 ka), (b) 6 ka, (c) 10 ka, and (d) LGM (21 ka). White areas indicate that no wetland area was simulated at this grid cell.

vegetation recorded in the paleorecord [*Hoelzmann et al.*, 1998]; this may be because the dynamic interplay between Holocene sea surface temperatures, land surface conditions, and the recycling of precipitation necessary to produce the vegetation shift could not be fully captured by the HC-UM GCM simulations [*Harrison et al.*, 1998].

3.2. Wetland Area and CH_4 Emissions

[32] The evolution of wetland areas from the LGM to the present is related to both the development of boreal peatlands on formerly glaciated areas, and the submergence of wetlands on both tropical and boreal continental shelves that were exposed at the LGM. While total global wetland area decreased slightly between the LGM and preindustrial, CH_4 emissions remained relatively constant over this time, with only a small maximum during the late Pleistocene (Figure 3). The change in global CH_4 emissions is caused by the simultaneous decrease in area of dominant tropical sources, and the overall increase in CH_4 emissions due to warmer and wetter global climate and higher CO_2 concentrations that stimulated vegetation productivity.

[33] In our simulations for the preindustrial, global wetlands mainly appear in tropical and boreal lowland regions, with their largest extents in the Amazon basin and western Siberia, respectively. Other major wetland areas occur in the Pantanal of southern South America, in boreal North America, Eastern Europe, and in the Congo basin and Indonesian lowlands (Figure 4a). Total global wetland area at the preindustrial is calculated to amount to 5.8×10^6 km^2, which is within the range of other estimates, although these figures vary widely even for the present day [*Kaplan*, 2002]. BIOME4-TG probably underestimates the concentration of wetland area in boreal Canada and specifically in the Hudson Bay Lowlands (HBL). However, recent studies suggest that the HBL is a relatively small CH_4 source ($\sim$0.5 Tg yr^{-1}) when integrated over the whole region [*Roulet et al.*, 1994; *Worthy et al.*, 2000]. We therefore expect that the underestimate of Canadian wetland area by BIOME4-TG does not affect global CH_4 emissions or their geographic distribution significantly.

[34] At the LGM, wetlands were greatly reduced from their current extent in North America, Europe and western Siberia because of the presence of the ice sheets and perennially frozen soils (Figure 4d). Large wetland areas are simulated on the exposed continental shelves, however, particularly in Beringia, and on the tropical Sunda and Gulf of Carpenteria shelves. Total global wetland area at the LGM is simulated at 6.8×10^6 km^2, slightly more than at preindustrial, but within the uncertainty of present-day estimates.

[35] From the LGM to the early Holocene (circa 12 ka), wetland area remained relatively constant and then decreased slightly through the course of the Holocene. At 10 ka wetlands are seen occupying much of western Siberia

Table 2. Comparison of Best Estimates for BVOC Surface Emissions as Calculated by BIOME4-TG and Published in Two Comparable Recent Studies[a]

	PIH	6 ka	10 ka	LGM
		Isoprene		
This study	541	516	539	335
Adams et al. [2001]	561	666	677	383
Valdes et al. [2005]	594			229
		Terpene		
This study	121	118	112	80
Adams et al. [2001]	116	137	137	99
Valdes et al. [2005]	97			55
		ORVOC		
This study	183	174	166	121
Adams et al. [2001]	226	286	290	161
Valdes et al. [2005]	335			224
		Total BVOC		
This study	845	808	817	536
Adams et al. [2001]	903	1089	1104	643
Valdes et al. [2005]	1026			508

[a]Emissions are given in Tg C yr^{-1}.

and Europe near preindustrial extent, while some wetland area still remained on the exposed remnants of Beringia and the Sunda shelf, and most of the boreal eastern North America was under glacial ice (Figure 4c). At 6 ka, with the final melting of the Laurentide ice sheet and the stabilization of sea level, wetland distribution is very similar to the preindustrial (Figure 4b).

[36] In contrast to the decrease in wetland area, CH_4 emissions from wetlands were similar at LGM and the preindustrial, with a value of ~110 Tg yr^{-1} (Figure 3). During the late Pleistocene, CH_4 emissions reached a maximum. At all time slices, however, global CH_4 emissions are within the range estimates for the present day [*Kaplan*, 2002], although seasonal and interannual variability may have been much more pronounced at times before the PIH (J. O. Kaplan, unpublished results, 2005). Global CH_4 emissions are dominated by tropical wetland sources in these simulations, and so the evolution and submergence of boreal wetlands during the course of the deglaciation only has a secondary effect on the global total.

[37] The late Pleistocene maximum in wetland CH_4 emissions occurs when a significant part of the tropical continental shelves were still exposed, while increasing precipitation due to warmer sea surface temperatures, and increased atmospheric CO_2 concentrations had a strong effect on vegetation productivity and carbon turnover. As sea level stabilized near present levels, and shallow continental shelves were submerged, CH_4 emissions from wetlands gradually decreased to near-preindustrial levels.

[38] Uncertainty in estimates of global wetland CH_4 emissions for the present day is large. While the total budget of CH_4 is well constrained by atmospheric measurement, a twofold range in the magnitude of global wetland CH_4 sources has been proposed by different studies [see *Kaplan*, 2002], though most studies converge in a range of ±20% of the mean. In the past we may expect somewhat greater uncertainty. While the processes of CH_4 formation in wetlands are identical, long-term changes in soils, topography, and CO_2 concentration may all effect net CH_4 emissions. We estimate that a doubling or halving of the global CH_4 emissions in our paleoscenarios would be within the range of uncertainty in model parameterizations and assumptions, although we do not expect the direction of change relative to PIH to be different. Future research should attempt full sensitivity analysis to better quantify the impact of these uncertainties on the composition of paleoatmospheres.

3.3. BVOC Emissions

[39] Table 2 summarizes BVOC surface flux simulated by BIOME4-TG at the four key time periods considered in the chemistry-climate model runs, along with estimates of BVOC emissions from other recent studies. In our simulations, total global BVOC emissions increased steadily from 21 ka to the preindustrial, with an LGM minimum of 625 Tg yr^{-1} and a preindustrial value of 1050 Tg yr^{-1} (Figure 3). BVOC emissions do show an early Holocene maximum with values at 10 ka near those for the preindustrial, a slight decrease to 6 ka, followed by recovery to near present-day levels.

[40] Our estimates of total global BVOC flux are consistent with *Adams et al.* [2001] and *Valdes et al.* [2005], though they differ by up to 30% for individual species. All estimates virtually agree on preindustrial emissions of isoprene and terpenes, but diverge more pronouncedly at the earlier periods, with the calculations of *Adams et al.* [2001] 15% to 30% higher, and *Valdes et al.* [2005] lower by similar magnitude. Larger differences arise for ORVOC emissions, which in our case are somewhat lower than the other estimates (between 25% at PI and 75% at 10 ka).

[41] Because of the short lifetime of BVOCs, the geographic distribution of emissions is as important as the total flux and the species composition. Over the last 21 ka the global pattern of BVOC emissions changes (Figure 5) for two major reasons: (1) the establishment of temperate and boreal vegetation after deglaciation and (2) the in situ enhancement of tropical sources stimulated by increased humidity and CO_2 fertilization.

[42] Ice sheet retreat and the subsequent development of cold needleleaf forests (Figure 2) resulted in the appearance of BVOC emissions from areas that had little or no emissions at the LGM. Temperate forest development also resulted in increased BVOC fluxes over eastern North America, Europe, and northeast Asia. Tropical BVOC emissions, which are significantly larger in overall magnitude than boreal or temperate sources, largely intensified in situ in response to the increased humidity and CO_2 concentrations that accompanied deglaciation. As noted in previous sections, the increase in some areas of tropical forests (e.g., in South America) was offset by the inundation of other regions (e.g., on the Sunda Shelf), which led to a meridional redistribution of tropical BVOC sources.

[43] The geographic changes in BVOC emissions are also apparent in the temporal pattern of the species distribution

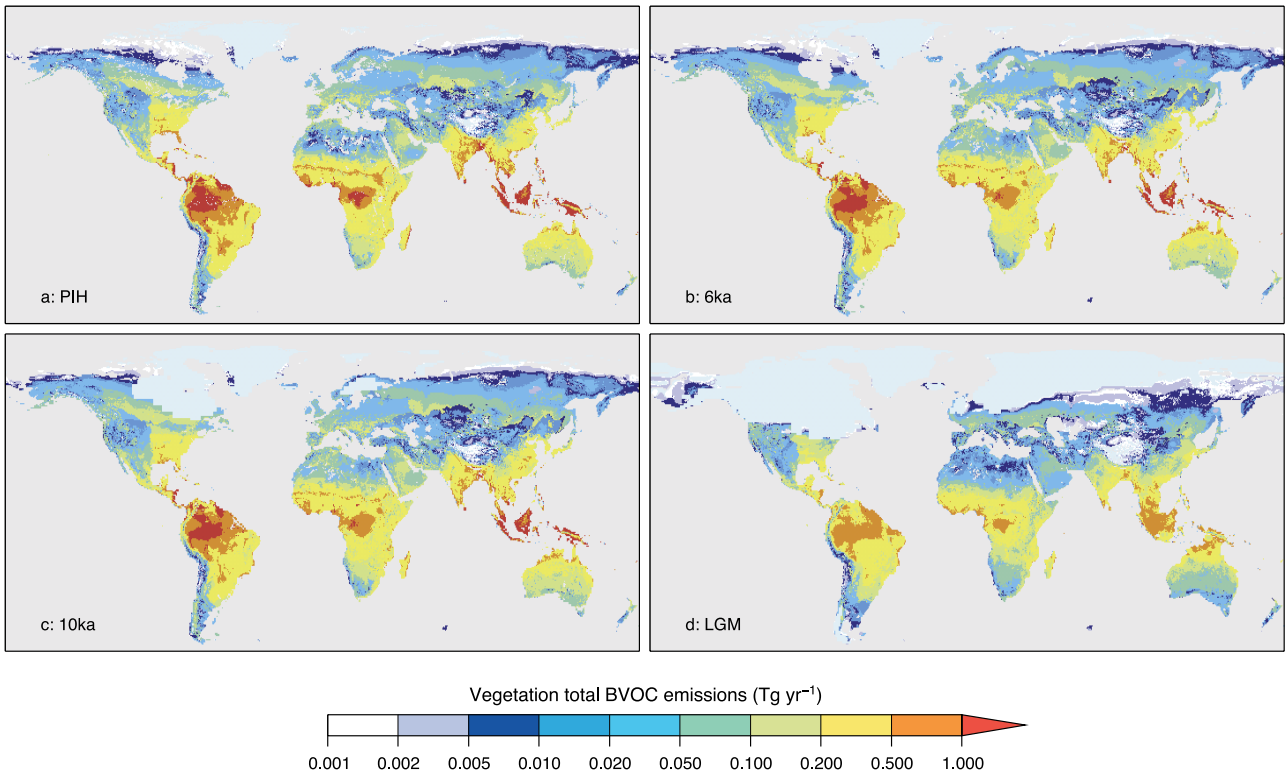

Figure 5. Global distribution of total annual BVOC emissions from terrestrial vegetation simulated by BIOME4-TG at (a) the "preindustrial" (0 ka), (b) 6 ka, (c) 10 ka, and (d) LGM (21 ka).

of total BVOC (Figure 6). Isoprene, which is largely emitted by broadleaf vegetation in tropical and temperate forests, increased most strongly between 21 ka and 10 ka, when the effect of CO_2 fertilization and increasing humidity would have been strongest. In contrast, terpene emissions, which are greatest in needleleaf forests such as those in cold biomes, increased steadily to the present because of the slow development of boreal forests in deglaciated regions, and somewhat less so by the nonuniform effect of warmer temperatures in the high latitudes. Methanol

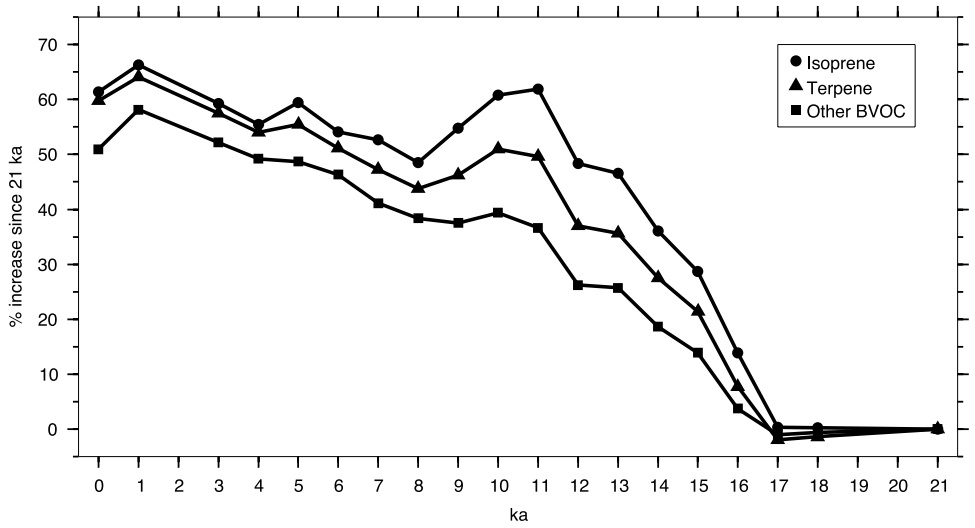

Figure 6. Time series plot of the percent increase in emissions relative to LGM of the BVOC species isoprene, terpene, and other BVOC simulated by BIOME4-TG.

Table 3. Atmospheric Burdens of CO, O_3, OH, and the CH_4 Lifetime Simulated by LMDz-INCA at the Four Representative Time Slices

Time	CO, Tg	O_3, Tg	OH, 10^5 cm^{-3}	CH_4 Lifetime, years
PIH	165.9	199.1	10.1	9.35
6 ka	140.2	192.9	10.8	8.73
10 ka	139.7	192.6	10.7	8.80
LGM	87.7	137.6	12.9	7.28

fluxes (included in other BVOC) originate primarily from grasslands [*Galbally and Kirstine*, 2002; *Kirstine et al.*, 1998; *Warneke et al.*, 1999], and also increased over the entire period of deglaciation and throughout the Holocene. Increase in these fluxes is related to the increase in the productivity of global grasslands as a result of climate warming and increased atmospheric CO_2 concentrations.

[44] In all of our calculations of BVOC emissions substantial uncertainties exist, not in the least because of the uncertainty in present-day estimates of VOC emissions rates from global terrestrial vegetation. Simulations of the global BVOC surface flux by vegetation models is affected by uncertainty in our simulation of vegetation distribution and climatic parameters controlling BVOC emissions (e.g., surface solar radiation and canopy deposition), as well as biological factors not considered in the vegetation model (e.g., herbivory and disease) [*Guenther et al.*, 1995]. Because of the large measured plant-interspecific variation in BVOC emissions, the use of plant functional types in our model represents an additional simplification and adds to the uncertainty in our calculations. The assumption that VOC emission rates at conditions prevailing at the LGM and the interglacial periods are comparable to emission rates derived for present-day conditions remains unverifiable.

[45] For the present day, landscape-averaged emission factors for isoprene and monoterpene in similar ecosystems vary ~fivefold [*Guenther et al.*, 1995]. OVOC emission factors are much more uncertain, and could vary up to 100 times among species [*Guenther et al.*, 1995; *MacDonald and Fall*, 1993]. This wide variability in measured emission factors could lead to uncertainty in the total global BVOC flux on the order of ±100%. On the other hand, plausible upper and lower limits for global BVOC emissions may be estimated from measurements of key atmospheric species, for example, O_3 [*Folberth et al.*, 2005a]. Given relatively well-constrained budgets of well-mixed reactive trace gases for the present day [see, e.g., *Ramaswamy et al.*, 2001], we believe that our calculations are a valid approximation of the relative changes in total annual BVOC emissions from global terrestrial vegetation from the LGM to preindustrial times.

3.4. OH Concentrations and CH_4 Lifetimes

[46] Table 3 summarizes the global annual mean burdens of CO, tropospheric O_3 and OH, and the CH_4 lifetime simulated by LMDz-INCA at each of the four model time slices. The decrease in OH concentration from the LGM to PIH of 2.8×10^5 molecules/cm^3 (22%) is concomitant with increases of similar magnitude in CO and O_3 burden. Because surface emissions of CO were kept constant in the three paleo time slices in these experiments, apparent changes in CO burden are related to the changes in OH. These results, along with the decrease in O_3 over the same time period, illustrate the effect of changing BVOC emissions on the oxidizing capacity of the atmosphere from the LGM through the Holocene.

[47] The vast majority of CH_4 and BVOCs emitted by the terrestrial biosphere are oxidized in the gas phase through the reaction with OH. An increasing reactive carbon burden in the atmosphere will reduce OH abundance, especially in the highly NO_x limited atmosphere of the preindustrial eras. Given a relatively constant source of CH_4 as simulated by BIOME4-TG, the change in the ratio of CH_4 to other RCCs drove the increase in CH_4 lifetime from LGM to preindustrial. This CH_4-to-other-RCC ratio decreased from 0.25 at LGM to about 0.19 at preindustrial. Correspondingly, the global annual mean photochemical lifetime of CH_4 increased by 2.1 years or about 29% from LGM (7.3 years) to preindustrial (9.4 years). The change in CH_4 lifetime is directly related to changes in its atmospheric concentration, as described in the following section.

[48] As noted above, our calculations of the changes in OH burden are based only on the change in surface emissions of reactive trace gases and do not include the effect of changes in climate, surface albedo, the stratospheric ozone column, or emissions of other reactive trace gases. These limitations are discussed below.

[49] Changes in the Earth's albedo from, for example, the presence or absence of sea ice and ice sheets, will have an effect on the global radiation budget. Ultraviolet (UV) radiation flux in the 290 to 310 nm range controls tropospheric ozone photolysis and therefore has a strong influence on OH burdens. However, studies by *Pinto and Khalil* [1991] and *Martinerie et al.* [1995, Figure 8] suggest that variations in the total ozone column between preindustrial and LGM were less than 2%. Even assuming that variations in stratospheric ozone were negligible [*Pinto and Khalil*, 1991], the impact of changing albedo on tropospheric chemistry is expected to be much smaller than the effect of changes in water vapor.

[50] The change in the water vapor content of the troposphere is a major contributor to the uncertainty of our model calculations. By repeating LGM model runs with preindustrial climate, *Valdes et al.* [2005] report a climate sensitivity of the global mean CH_4 concentration and OH burden on the order of 10% and 7%, respectively. Similarly, 2D chemistry-climate model experiments by *Martinerie et al.* [1995] suggested that lower water vapor during the LGM would decrease global OH concentration by 7%, resulting in an increase of CH_4 lifetime by 6%. On the other hand, uncertainty in regional climate change itself between LGM and PIH remains large, particularly for important parameters that influence tropospheric water vapor content, for example, tropical temperatures [*Farrera et al.*, 1999; *Pinot et al.*, 1999].

[51] Another source of uncertainty in the chemistry-climate model experiments is the potential for long-term changes in the production of NO_x by lightning. To inves-

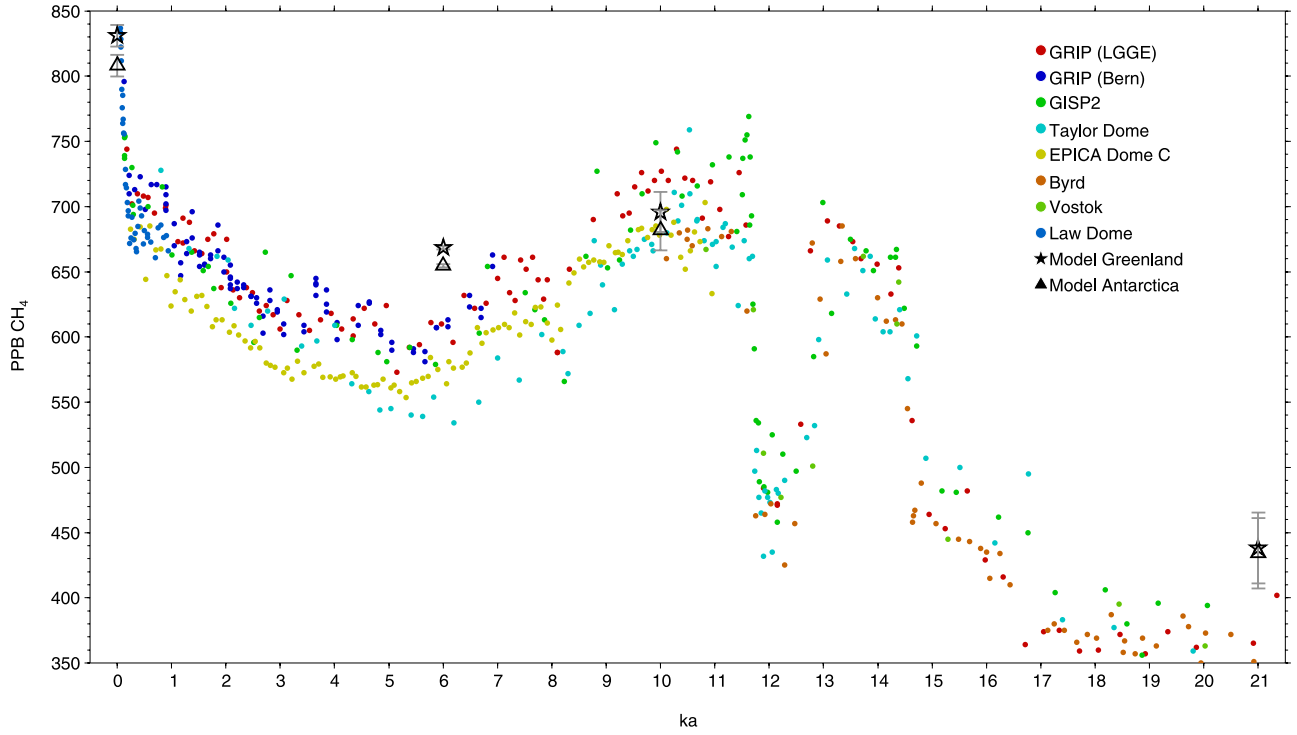

Figure 7. Atmospheric CH_4 concentrations measured in Greenland and Antarctic ice cores and simulated by BIOME4-TG–LMDz-INCA. Error bars in modeled concentrations represent 1σ variation in interannual and seasonal variability. Measured CH_4 concentrations are from data archived at the World Data Center for Paleoclimatology, Boulder, Colorado [*Blunier et al.*, 1993, 1995; *Brook et al.*, 2000; *Chappellaz et al.*, 1990, 1993a; *Flückiger et al.*, 2002; *Raynaud et al.*, 1988].

tigate this possibility, we analyzed global fields of convective precipitation rate (a diagnostic for lightning abundance) in the output of the HC-UM paleoclimate simulations. Over the full 21 ka, no significant trend in convective precipitation rate could be identified; we therefore expect any changes in lightning-produced NO_x to have been small. Furthermore, the sensitivity analyses of *Valdes et al.* [2005] and those in previous studies [*Sinha and Toumi*, 1997; *Thompson et al.*, 1993] indicate that variation in NO_x appears to be a minor component in influencing the OH and CH_4 budget.

[52] Finally, the direct effect of tropospheric O_3 concentrations on plant productivity, while well known [*Gregg et al.*, 2003], was not included in this study. It is conceivable that reduced O_3, simulated here at all times before the PIH, could have led to an enhancement of overall vegetation productivity and hence BVOC emissions. While the effect is probably small, investigation of such feedback would be an important question for future research.

[53] Changes in climate and land surface conditions could counteract up to one third of the 22% change in OH burden between LGM and PIH we simulate here. Nevertheless, it is clear that changing BVOC emissions have a significant impact on tropospheric chemistry and CH_4 lifetimes. Further research and sensitivity analysis with 3D chemistry-climate models will be required to better quantify the importance of individual uncertainties, all of which contribute to the mismatch between modeled and measured CH_4 concentrations.

3.5. Modeled and Ice Core Measured Atmospheric CH_4 Concentrations

[54] In Figure 7 the atmospheric CH_4 concentrations simulated by LMDz-INCA are plotted together with measured CH_4 concentrations sampled from several ice cores from Greenland and Antarctica. Measured atmospheric CH_4 concentrations increased by about 450 ppb from LGM to preindustrial, with a rapid increase during the deglaciation, and a relative minimum in the mid-Holocene (∼6 ka). Modeled atmospheric CH_4 concentrations increase ∼385 ppb between LGM and PIH and are within 15% of the measurements at all time slices.

[55] We expect discrepancies between measured and modeled CH_4 concentrations in these experiments. As described in previous sections, each component of the linked model simulations that ultimately govern CH_4 concentrations has errors related to uncertainties and assumptions in the model setup. Nevertheless, the close agreement between model and measurements in these experiments demonstrates that changing BVOC emissions are a decisive factor in the CH_4 cycle that is, for example, more important than the direct effect of climate change on photochemistry and OH burden. Our results support recent hypotheses that Glacial-Interglacial changes in atmospheric CH_4 concentra-

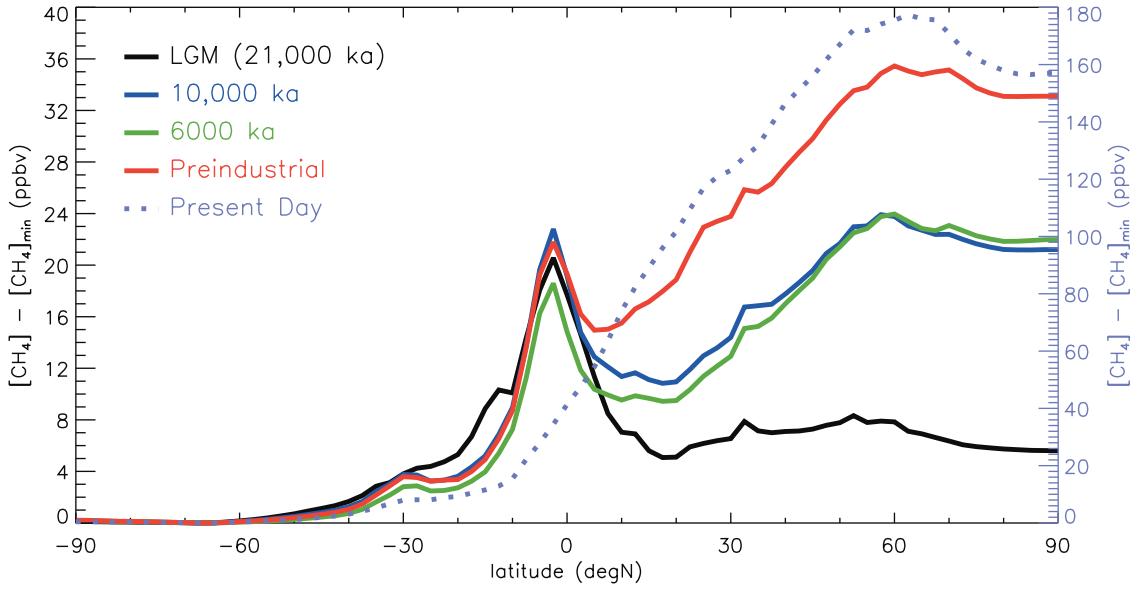

Figure 8. Zonal mean plot of atmospheric CH_4 concentrations simulated by LMDz-INCA at each of the four representative time slices.

tions could have been driven primarily by changes in the photochemical sink for CH_4 rather than changes in the source [*Adams et al.*, 2001; *Valdes et al.*, 2005].

[56] The Holocene record of atmospheric CH_4 concentrations bears further examination. Despite the relatively stable climate over this time period, CH_4 concentrations show a marked long-term trend, with an early Holocene maximum followed by a minimum around 6 ka and a steady increase to PIH. Modeled CH_4 concentrations are higher at both 10 ka and PIH than 6 ka. The early Holocene maximum in CH_4 concentrations is a reflection of the maximum in wetland CH_4 emissions, which decreased ~20% between 10 ka and 6 ka. At 6 ka, lower wetland CH_4 emissions effected lower atmospheric CH_4 concentrations despite the steady increase in BVOC emissions, as evidenced by the relatively stable OH burden over this time period (Table 3).

[57] Between 6 ka and PIH, the 15% and 30% respective anthropogenic increases in the CH_4 and CO inventories used in our experiments apparently have an effect on atmospheric CH_4. These results may support the recent hypothesis that early anthropogenic activity was a driver for the observed increase in atmospheric CH_4 concentrations over the past 6 ka [*Ruddiman and Thomson*, 2001]. It is likely, however, that areas of prehistoric rice cultivation were on floodplain wetlands, and that areas of anthropogenic CH_4 emissions supplanted areas of natural wetland emissions. This effect was not considered in this study and further research is needed to quantify the potential effect.

[58] Unfortunately, in these simulations we were not able to test mechanisms to explain rapid changes in atmospheric CH_4 observed in ice cores. We speculate that time-discrete mechanisms, such as the rapid inundation of tropical continental shelves and in situ decay of organic matter, concomitant with the long-term changes in the CH_4 sink, could explain the observation of rapid but permanent changes in atmospheric CH_4 concentrations. Further study with fully coupled land surface atmospheric chemistry models will be necessary in order to resolve remaining questions regarding the mismatch between model and observations.

3.6. CH_4 Interhemispheric Gradients

[59] Evaluation of the interhemispheric gradient in atmospheric CH_4 at times in the past is possible because of the existence of ice cores in the high latitudes of both hemispheres. These interhemispheric gradients may be used to imply temporal changes in the geographic distribution of CH_4 sources and sinks. In contrast to CH_4, which is relatively well mixed in the atmosphere, the short lifetimes of BVOCs mean that their effect on OH is mostly local. Therefore it is instructive to compare model simulations of the interhemispheric gradient in CH_4 to ice core records as a way of deducing the temporal variability in the interplay of CH_4 sources and sinks.

[60] Figure 8 shows normalized interhemispheric gradients of zonally averaged atmospheric CH_4 concentrations at each time slice of our model simulations and for the present-day simulation of LMDz-INCA (note the different scale in Figure 8 for the CH_4 gradient at present-day conditions because of the predominance of anthropogenic sources). The gradients were derived by calculating zonal means of the annually averaged CH_4 concentration at the lowest model level at each time slice and normalizing these values by subtracting the minimum CH_4 concentration for each time slice individually. In all cases, the minimum in atmospheric CH_4 occurs at approximately the same latitude (~70°S). The appearance of the minima at this latitude is due to the absence of CH_4 sources in the high latitudes of the Southern Hemisphere. Poleward of the minimum, very low OH concentrations yield somewhat longer CH_4 life-

times and hence marginally higher concentrations. Northward of the minimum, both surface fluxes and OH burdens increase, though with substantially different patterns at the different time slices.

[61] At LGM, the CH_4 gradient is nearly symmetric around the equator with a strong peak in the tropics due to the predominance of CH_4 sources in tropical latitudes (Figure 4). Low temperatures and widespread areas of ice, tundra, and cold forests (Figure 3) led to relatively low extratropical BVOC production, resulting in short CH_4 lifetimes and low concentrations at northern and southern midlatitudes to high latitudes. The interpolar difference (IPD) [*Dällenbach et al.*, 2000] in CH_4 concentrations simulated by the model is 4 ± 4 ppb, which is comparable to the ice core LGM mean of -3 ± 4 measured by *Dällenbach et al.* [2000] and somewhat smaller than the 18 ± 7 reported by *Brook et al.* [2000], though it must be noted that both of these measurements represent integrations of some thousand years around 21 ka.

[62] During the late Pleistocene and early Holocene the CH_4 gradients show an increasingly asymmetric shape with an evolving second peak at northern midlatitudes to high latitudes ($\sim$60°N). We attribute the evolution of the asymmetry in the CH_4 gradient over time to both the development of boreal wetlands after deglaciation, and the increase in BVOC emissions in the Northern Hemisphere and the consequent reduction in the strength of the photochemical CH_4 sink. Measurements of the IPD over this time period were approximately 44 ± 4 ppb [*Chappellaz et al.*, 1997; *Dällenbach et al.*, 2000], while the model simulates a substantially smaller IPD of only 14 ± 6 ppb. The origin of this model-data mismatch may be due to the omission of circulation-related climate changes in the LMDz-INCA model simulations and highlights a limitation of our modeling approach. The transport simulated by LMDz-INCA has been extensively validated for present-day conditions, both with passive tracers and for CH_4 itself [*Folberth et al.*, 2005a; *Hauglustaine et al.*, 2004]. However, different boundary conditions between PIH and 10 ka and 6 ka, particularly regarding solar forcing and the intrahemispheric temperature gradient, may have resulted in significantly increased latitudinal atmospheric transport relative to the PIH. While it is also possible that we underestimate the magnitude and development of boreal CH_4 sources in BIOME4-TG, recent syntheses of global methane sources indicate the general predominance of wetland CH_4 emissions from the tropics [*Frankenberg et al.*, 2005].

[63] At the PIH, northern midlatitudinal and high-latitudinal CH_4 concentrations surpass the extant tropical peak in magnitude. Additional anthropogenic CH_4 sources from landfills and rice cultivation, along with a decreasing sink for CH_4 effected by increasing BVOC emissions, added to the buildup of the Northern Hemisphere midlatitudinal maximum.

[64] Under present-day conditions, the tropical maximum appears to disappear entirely because of the abundance of anthropogenic sources of CH_4 and photochemical CH_4 precursors, which are strongly biased to the Northern Hemisphere. The shape of the interhemispheric gradients in the Southern Hemisphere suggests that southern hemispheric CH_4 concentrations are dominated by atmospheric transport rather than direct sources.

4. Conclusions

[65] To assess the effect of changing emissions of different reactive trace gases on atmospheric CH_4 concentrations, we performed a series of vegetation model simulations that included process-based estimates of CH_4 emissions from wetlands and BVOC emissions from all vegetation at 1000-year intervals from 21 ka to the present. While wetland CH_4 emissions were relatively stable over the course of the late Pleistocene and Holocene, BVOC emissions from vegetation nearly doubled over this time period. At four key time slices we linked the vegetation model output to an atmospheric chemistry climate model to directly simulate the burden of the OH sink, the resulting CH_4 concentrations, and the interhemispheric gradient in CH_4.

[66] While the rapid changes in atmospheric CH_4 concentrations observed in ice cores over the past 21 ka cannot be attributed to climate change on millennial timescales, our results indicate that significant, permanent changes in CH_4 concentrations could have been a result of the doubling in BVOC emissions that occurred over this time period, through the competition with CH_4 for the OH sink. With stable wetland CH_4 emissions, this interplay between the reactive trace gases could have increased CH_4 concentrations by $\sim$385 ppb at the present as compared to the LGM and have been responsible for much of the observed Holocene variability in atmospheric CH_4 concentrations.

[67] The evolution of the emission inventories of CH_4 and BVOC calculated by BIOME4-TG together with the interhemispheric CH_4 gradient calculated by LMDz-INCA illustrates that the change in the atmospheric CH_4 concentrations was the result of the geographic redistribution of both sources and sinks. In the tropics, decreasing wetland CH_4 emissions combined with an increase in BVOC sources led to only a small net increase in CH_4 concentrations. In the Northern Hemisphere extratropics, the development of wetland CH_4 sources combined with increasing BVOC emissions led to strong increases in CH_4 concentrations. This picture is consistent with the asymmetrical increase in the interpolar difference in atmospheric CH_4 concentrations documented in the ice core record.

[68] The study presented here has some important limitations, the most prominent of which is the disregard of changing climate in our chemistry-climate modeling experiments. The stratospheric ozone column, and hence the low-energy UV flux, as well as the surface albedo were kept identical to the preindustrial control run; this may have a particularly important effect on global OH concentrations. Nevertheless, we consider our work to be an important sensitivity study that highlights the significance of potential changes in the sink for CH_4 as a mechanism for explaining long-term changes in atmospheric CH_4. To gain a more thorough understanding of the processes that governed the increase in atmospheric CH_4 concentrations over the last 21 ka, it will be necessary to account for climate change in chemistry-climate model runs, and to perform annually

resolved transient model runs over times of century-scale rapid climate change.

[69] **Acknowledgments.** This work was partly supported by the European Commission under contracts EVK2-CT-1999-0030 and EVK2-CT-1999-00021 and a Marie Curie Fellowship to JOK. GF and JOK acknowledge support by the Canadian Centre for Climate Modeling and Analysis, Meteorological Service of Canada, the GCC project, NSERC, and CFCAS. This work was partly supported by the French national program ECLIPSE al LSCE. We are grateful for computing help from Charles Audiffren and resources from the Commissariat à l'Energie Atomique under project p24 and publication support from the Geobotanik Fonds of the University of Bern. We thank the editor and two anonymous reviewers for their valuable comments, which improved this manuscript.

References

Adams, J. M., J. V. H. Constable, A. B. Guenther, and P. Zimmerman (2001), An estimate of natural volatile organic compound emissions from vegetation since the last glacial maximum, *Chemosphere*, *3*, 73–91.

Berger, A., M.-F. Loutre, and C. Tricot (1993), Insolation and Earth's orbital periods, *J. Geophys. Res.*, *98*(D6), 10,341–10,362.

Bigelow, N. H., et al. (2003), Climate change and Arctic ecosystems: 1. Vegetation changes north of 55°N between the last glacial maximum, mid-Holocene, and present, *J. Geophys. Res.*, *108*(D19), 8170, doi:10.1029/2002JD002558.

Blunier, T., J. A. Chappellaz, J. Schwander, J.-M. Barnola, T. Desperts, B. Stauffer, and D. Raynaud (1993), Atmospheric methane from a Greenland ice core over the last 1000 years, *Geophys. Res. Lett.*, *20*, 2219–2222.

Blunier, T., J. A. Chappellaz, J. Schwander, B. Stauffer, and D. Raynaud (1995), Variations in atmospheric methane concentration during the Holocene epoch, *Nature*, *374*, 46–49.

Brook, E. J., T. Sowers, and J. Orchardo (1996), Rapid variations in atmospheric methane concentration during the past 110,000 years, *Science*, *273*, 1087–1091.

Brook, E. J., S. Harder, J. Severinghaus, E. J. Steig, and C. M. Sucher (2000), On the origin and timing of rapid changes in atmospheric methane during the last glacial period, *Global Biogeochem. Cycles*, *14*(2), 559–572.

Chappellaz, J. A., J.-M. Barnola, D. Raynaud, Y. S. Korotkevich, and C. Lorius (1990), Ice core record of atmospheric methane over the past 160000 years, *Nature*, *345*, 127–131.

Chappellaz, J. A., T. Blunier, D. Raynaud, J.-M. Barnola, J. Schwander, and B. Stauffer (1993a), Synchronous changes in atmospheric CH_4 and Greenland climate between 40 and 8 kyr B. P., *Nature*, *366*, 443–445.

Chappellaz, J. A., I. Y. Fung, and A. M. Thompson (1993b), The atmospheric CH_4 increase since the Last Glacial Maximum (1). Source estimates, *Tellus, Ser. B*, *45*(3), 228–241.

Chappellaz, J., T. Blunier, S. Kints, A. Dallenbach, J.-M. Barnola, J. Schwander, D. Raynaud, and B. Stauffer (1997), Changes in the atmospheric CH_4 gradient between Greenland and Antarctica during the Holocene, *J. Geophys. Res.*, *102*(D13), 15,987–15,997.

Christensen, T. R., I. C. Prentice, J. Kaplan, A. Haxeltine, and S. Sitch (1996), Methane flux from northern wetlands and tundra: An ecosystem source modelling approach, *Tellus, Ser. B*, *48*(5), 652–661.

CLIMAP Project Members (1976), The surface of the Ice-Age Earth, *Science*, *191*, 1131–1137.

CLIMAP Project Members (1981), Seasonal reconstructions of the Earth's surface as the Last Glacial Maximum, *Geol. Soc. Am. Map Chart Ser. 36*, Boulder, Colo.

Cowling, S. A., M. A. Maslin, and M. T. Sykes (2001), Paleovegetation simulations of lowland Amazonia and implications for neotropical allopatry and speciation, *Quat. Res.*, *55*(2), 140–149.

Crutzen, P. J., and C. Bruhl (1993), A model study of atmospheric temperatures and the concentrations of ozone, hydroxyl, and some other photochemically active gases during the glacial, the preindustrial Holocene and the present, *Geophys. Res. Lett.*, *20*(11), 1047–1050.

Dällenbach, A., T. Blunier, J. Flückiger, B. Stauffer, J. Chappellaz, and D. Raynaud (2000), Changes in the atmospheric CH_4 gradient between Greenland and Antarctica during the Last Glacial and the transition to the Holocene, *Geophys. Res. Lett.*, *27*(7), 1005–1008.

de Noblet, N. I., C. Prentice, S. Joussaume, D. Texier, A. Botta, and A. Haxeltine (1996), Possible role of atmosphere-biosphere interactions in triggering the last glaciation, *Geophys. Res. Lett.*, *23*(22), 3191–3194.

Dufresne, J.-L., L. Fairhead, H. Le Treut, M. Berthelot, L. Bopp, P. Ciais, P. Friedlingstein, and P. Monfray (2002), On the magnitude of positive feedback between future climate change and the carbon cycle, *Geophys. Res. Lett.*, *29*(10), 1405, doi:10.1029/2001GL013777.

Dyke, A. S., and V. K. Prest (1987), The late Wisconsin and Holocene history of the Laurentide Ice Sheet, *Geogr. Phys. Quat.*, *41*(2), 237–263.

Farrera, I., et al. (1999), Tropical climates at the Last Glacial Maximum: A new synthesis of terrestrial palaeoclimate data. I. Vegetation, lake levels and geochemistry, *Clim. Dyn.*, *15*(11), 823–856.

Flückiger, J., E. Monnin, B. Stauffer, J. Schwander, T. F. Stocker, J. Chappellaz, D. Raynaud, and J. Barnola (2002), High-resolution Holocene N_2O ice core record and its relationship with CH_4 and CO_2, *Global Biogeochem. Cycles*, *16*(1), 1010, doi:10.1029/2001GB001417.

Folberth, G., D. Hauglustaine, J. Lathiere, and F. Brocheton (2005a), Impact of biogenic hydrocarbons on tropospheric chemistry; results from a global chemistry-climate model, *Atmos. Chem. Phys. Discuss.*, *5*, 10,517–10,612.

Folberth, G., D. A. Hauglustaine, P. Ciais, and J. Lathière (2005b), On the role of atmospheric chemistry in the global CO_2 budget, *Geophys. Res. Lett.*, *32*, L08801, doi:10.1029/2004GL021812.

Frankenberg, C., J. F. Meirink, M. van Weele, U. Platt, and T. Wagner (2005), Assessing methane emissions from global space-borne observations, *Science*, *308*, 1010–1014.

Friedlingstein, P., L. Bopp, P. Ciais, J.-L. Dufresne, L. Fairhead, H. Le Treut, P. Monfray, and J. Orr (2001), Positive feedback between future climate change and the carbon cycle, *Geophys. Res. Lett.*, *28*(8), 1543–1546.

Galbally, I. E., and W. Kirstine (2002), The production of methanol by flowering plants and the global cycle of methanol, *J. Atmos. Chem.*, *43*(3), 195–229.

Gregg, J. W., C. G. Jones, and T. E. Dawson (2003), Urbanization effects on tree growth in the vicinity of New York City, *Nature*, *424*, 183–187.

Guenther, A., et al. (1995), A global model of natural volatile organic compound emissions, *J. Geophys. Res.*, *100*(D5), 8873–8892.

Harrison, S. P. (2000), Paleoenvironmental data sets and model evaluation in PMIP, paper presented at Paleoclimate Modeling Intercomparison Project (PMIP), World Clim. Res. Prog., World Meteorol. Org., La Huardière, Que., Canada.

Harrison, S. P., I. C. Prentice, and P. J. Bartlein (1992), Influence of insolation and glaciation on atmospheric circulation in the North Atlantic sector: Implications of general circulation model experiments for the late Quaternary climatology of Europe, *Quat. Sci. Rev.*, *11*, 283–299.

Harrison, S. P., et al. (1998), Intercomparison of simulated global vegetation distributions in response to 6 kyr BP orbital forcing, *J. Clim.*, *11*, 2721–2742.

Harrison, S. P., P. Braconnot, S. Joussaume, C. Hewitt, and R. J. Stouffer (2002), Comparison of palaeoclimate simulations enhances confidence in models, *Eos Trans. AGU*, *83*(40), 447.

Hauglustaine, D. A., F. Hourdin, L. Jourdain, M.-A. Filiberti, S. Walters, J.-F. Lamarque, and E. A. Holland (2004), Interactive chemistry in the Laboratoire de Météorologie Dynamique general circulation model: Description and background tropospheric chemistry evaluation, *J. Geophys. Res.*, *109*, D04314, doi:10.1029/2003JD003957.

Haxeltine, A., and I. C. Prentice (1996), BIOME3: An equilibrium terrestrial biosphere model based on ecophysiological constraints, resource availability, and competition among plant functional types, *Global Biogeochem. Cycles*, *10*(4), 693–709.

Hoelzmann, P., D. Jolly, S. P. Harrison, F. Laarif, R. Bonnefille, and H.-J. Pachur (1998), Mid-Holocene land-surface conditions in northern Africa and the Arabian peninsula: A data set for the analysis of biogeophysical feedbacks in the climate system, *Global Biogeochem. Cycles*, *12*(1), 35–51.

Hope, G., A. P. Kershaw, S. van der Kaars, S. Xiangjun, P.-M. Liew, L. E. Heusser, H. Takahara, M. McGlone, N. Miyoshi, and P. T. Moss (2004), History of vegetation and habitat change in the Austral-Asian region, *Quat. Int.*, *118–119*, 103–126.

Indermühle, A., et al. (1999), Holocene carbon-cycle dynamics based on CO_2 trapped in ice at Taylor Dome, Antarctica, *Nature*, *398*, 121–126.

Jolly, D., and A. Haxeltine (1997), Effect of low glacial atmospheric CO_2 on tropical African montane vegetation, *Science*, *276*, 786–788.

Kaplan, J. O. (2001), Geophysical applications of vegetation modeling, Ph.D. thesis, 132 pp., Lund Univ., Lund, Sweden.

Kaplan, J. O. (2002), Wetlands at the Last Glacial Maximum: Distribution and methane emissions, *Geophys. Res. Lett.*, *29*(6), 1079, doi:10.1029/2001GL013366.

Kaplan, J. O. (2006), Late Quaternary-Holocene vegetation modeling, in *Encyclopedia of Paleoclimatology and Ancient Environments*, edited by V. Gornitz, Springer, New York, in press.

Kaplan, J. O., I. C. Prentice, W. Knorr, and P. J. Valdes (2002), Modeling the dynamics of terrestrial carbon storage since the Last Glacial Maximum, *Geophys. Res. Lett.*, *29*(22), 2074, doi:10.1029/2002GL015230.

Kaplan, J. O., et al. (2003), Climate change and Arctic ecosystems: 2. Modeling, paleodata-model comparisons, and future projections, *J. Geophys. Res.*, *108*(D19), 8171, doi:10.1029/2002JD002559.

Kennett, J. P., K. G. Cannariato, I. L. Hendy, and R. J. Behl (2003), *Methane Hydrates in Quaternary Climate Change: The Clathrate Gun Hypothesis*, *Spec. Publ.*, vol. 54, edited by J. P. Kennett et al., 216 pp., AGU, Washington.

Kirstine, W., I. Galbally, Y. R. Ye, and M. Hooper (1998), Emissions of volatile organic compounds (primarily oxygenated species) from pasture, *J. Geophys. Res.*, *103*(D9), 10,605–10,619.

Lathière, J., D. A. Hauglustaine, A. Friend, N. de Noblet-Ducoudre, N. Viovy, and G. Folberth (2005), Impact of climate variability and land use changes on global biogenic volatile organic compound emissions, *Atmos. Chem. Phys. Discuss.*, *5*, 10,613–10,656.

Leemans, R., and W. P. Cramer (1991), The IIASA database for mean monthly values of temperature, precipitation, and cloudiness on a global terrestrial grid, 62 pp., Int. Inst. for Appl. Syst. Anal., Laxenberg, Austria.

Lelieveld, J., P. J. Crutzen, and F. J. Dentener (1998), Changing concentration, lifetime and climate forcing of atmospheric methane, *Tellus, Ser. B*, *50*(2), 128–150.

MacDonald, G. M., et al. (2000), Holocene treeline history and climate change across northern Eurasia, *Quat. Res.*, *53*(3), 302–311.

MacDonald, R., and R. Fall (1993), Detection of substantial emissions of methanol from plants to the atmosphere, *Atmos. Environ., Part A*, *27*, 1709–1713.

Martinerie, P., G. P. Brasseur, and C. Granier (1995), The chemical composition of ancient atmospheres: A model study constrained by ice core data, *J. Geophys. Res.*, *100*(D7), 14,291–14,304.

Mitchell, J. F. B., N. S. Grahame, and K. J. Needham (1988), Climate simulations for 9000 years before present: Seasonal variations and effect of the Laurentide ice sheet, *J. Geophys. Res.*, *93*(D7), 8283–8303.

Neftel, A., H. Oeschger, T. Staffelbach, and B. Stauffer (1988), CO_2 record in the Byrd ice core 50,000–5,000 years BP, *Nature*, *331*, 609–611.

Peltier, W. R. (1994), Ice Age paleotopography, *Science*, *265*, 195–201.

Petit, J. R., et al. (1999), Climate and atmospheric history of the past 420,000 years from the Vostok ice core, Antarctica, *Nature*, *399*, 429–436.

Pinot, S., G. Ramstein, S. P. Harrison, I. C. Prentice, J. Guiot, M. Stute, S. Joussaume, and PMIP Participating Groups (1999), Tropical paleoclimates at the Last Glacial Maximum: Comparison of Paleoclimate Modeling Intercomparison Project (PMIP) simulations and paleodata, *Clim. Dyn.*, *15*, 857–874.

Pinto, J. P., and M. A. K. Khalil (1991), The stability of tropospheric OH during ice ages, inter-glacial epochs and modern times, *Tellus, Ser. B*, *43*(5), 347–352.

Prentice, I. C. (2001), Last Glacial Maximum and Mid-Holocene vegetation: Data and models, *Nova Acta Leopold.*, *88*(331), 61–70.

Prentice, I. C., and T. Webb III (1998), BIOME 6000: Reconstructing global mid-Holocene vegetation patterns from palaeoecological records, *J. Biogeogr.*, *25*, 997–1005.

Prentice, I. C., D. Jolly, and BIOME 6000 Participants (2000), Mid-Holocene and glacial-maximum vegetation geography of the northern continents and Africa, *J. Biogeogr.*, *27*, 507–519.

Ramaswamy, V., O. Boucher, J. Haigh, D. Hauglustaine, J. Haywood, G. Myhre, T. Nakajima, G. Y. Shi, and S. Solomon (2001), Radiative forcing of climate change, in *Climate Change 2001: The Scientific Basis*, edited by J. T. Houghton et al., pp. 349–416, Cambridge Univ. Press, New York.

Raynaud, D., J. A. Chappellaz, J.-M. Barnola, Y. S. Korotkevich, and C. Lorius (1988), Climatic and CH_4 cycle implications of glacial-interglacial CH_4 change in the Vostok ice fore, *Nature*, *333*, 655–657.

Raynaud, D., J. Jouzel, J. M. Barnola, J. Chappellaz, R. J. Delmas, and C. Lorius (1993), The ice record of greenhouse gases, *Science*, *259*, 926–934.

Ritchie, J. C., L. C. Cwynar, and R. W. Spear (1983), Evidence from northwest Canada for an early Holocene Milankovitch thermal maximum, *Nature*, *305*, 126–128.

Roulet, N. T., A. Jano, C. A. Kelley, L. F. Klinger, T. R. Moore, R. Protz, J. A. Ritter, and W. R. Rouse (1994), Role of the Hudson Bay Lowland as a source of atmospheric methane, *J. Geophys. Res.*, *99*(D1), 1439–1454.

Ruddiman, W. F., and J. S. Thomson (2001), The case for human causes of increased atmospheric CH_4 over the last 5000 years, *Quat. Sci. Rev.*, *20*, 1769–1777.

Sadourny, R., and K. Laval (1984), January and July performance of the LMD general circulation model, in *New Perspectives in Climate Modelling*, edited by A. L. Berger and C. Nicolls, pp. 173–197, Elsevier, New York.

Schaefer, H. (2005), Stable carbon isotopic composition of methane from ancient ice samples, Ph.D. thesis, 191 pp., Univ. of Victoria, Victoria, B. C., Canada.

Sinha, A., and R. Toumi (1997), Tropospheric ozone, lightning, and climate change, *J. Geophys. Res.*, *102*(D9), 10,667–10,672.

Sitch, S., et al. (2003), Evaluation of ecosystem dynamics, plant geography and terrestrial carbon cycling in the LPJ dynamic global vegetation model, *Global Change Biol.*, *9*(2), 161–185.

Stauffer, B., et al. (1998), Atmospheric CO_2 concentration and millennial-scale climate change during the last glacial period, *Nature*, *392*, 59–62.

Svendsen, J. I., H. Alexanderson, V. I. Astakhov, I. Demidov, J. A. Dowdeswell, S. Funder, V. Gataullin, M. Henriksen, C. Hjort, and M. Houmark-Nielsen (2004), Late Quaternary ice sheet history of northern Eurasia, *Quat. Sci. Rev.*, *23*, 1229–1271.

Thompson, A. M., J. A. Chappellaz, I. Y. Fung, and T. L. Kucsera (1993), The atmospheric CH_4 increase since the Last Glacial Maximum (2). Interactions with oxidants, *Tellus, Ser. B*, *45*(3), 242–257.

Tiedke, M. (1989), A comprehensive mass-flux scheme for cumulus parameterization in large scale models, *Mon. Weather*, 1779–1800.

Transeau, E. N. (1935), The Prairie Peninsula, *Ecology*, *16*(3), 423–437.

Valdes, P. J., D. J. Beerling, and C. E. Johnson (2005), The ice age methane budget, *Geophys. Res. Lett.*, *32*, L02704, doi:10.1029/2004GL021004.

Van Leer, B. (1977), Towards the ultimate conservative difference scheme. Part IV: A new approach to numerical convection, *J. Comput. Phys.*, *23*, 276–299.

Walter, H. (1973), *Vegetation of the Earth in Relation to Climate and the Eco-Physiological Conditions*, Springer, New York.

Walter, H., E. Harnickell, and D. Mueller-Dombois (1975), *Climate-Diagram Maps*, 36 pp., Springer, New York.

Warneke, C., T. Karl, H. Judmaier, A. Hansel, A. Jordan, W. Lindinger, and P. J. Crutzen (1999), Acetone, methanol, and other partially oxidized volatile organic emissions from dead plant matter by abiological processes: Significance for atmospheric HO_x chemistry, *Global Biogeochem. Cycles*, *13*(1), 9–17.

Worthy, D. E. J., I. Levin, F. Hopper, M. K. Ernst, and N. B. A. Trivett (2000), Evidence for a link between climate and northern wetland methane emissions, *J. Geophys. Res.*, *105*(D3), 4031–4038.

Yienger, J. J., and H. Levy II (1995), Empirical model of global soil-biogenic NO_x emissions, *J. Geophys. Res.*, *100*(D6), 11,447–11,464.

G. Folberth, School of Earth and Ocean Sciences, University of Victoria, P.O. Box 3055 STN CSC, Victoria, BC, Canada V8W 3P6. (gerd.folberth@ec.gc.ca)

D. A. Hauglustaine, Laboratoire des Sciences du Climat et de l'Environnement, CEN Saclay, Orme des Merisiers, Bat. 701, F-91191 Gif-sur-Yvette Cedex, France. (didier.hauglustaine@cea.fr)

J. O. Kaplan, Institute of Plant Sciences, University of Bern, Altenbergrain 21, CH-3013 Bern, Switzerland. (jed.kaplan@ips.unibe.ch)